Heliyon 9 (2023) e15556

Contents lists available at ScienceDirect

Heliyon

journal homepage: www.cell.com/heliyon

Research article

Distinctions in bone matrix nanostructure, composition, and formation between osteoblast-like cells, MG-63, and human mesenchymal stem cells, UE7T-13

Kamonwan Chatree [a], Patsawee Sriboonaied [a], Chinnatam Phetkong [a], Witoon Wattananit [b], Chanpen Chanchao [c], Adisri Charoenpanich [a,*]

[a] Department of Biology, Faculty of Science, Silpakorn University, Nakhon Pathom, Thailand
[b] Scientific and Technological Equipment Centre, Faculty of Science, Silpakorn University, Nakhon Pathom, Thailand
[c] Department of Biology, Faculty of Science, Chulalongkorn University, Bangkok, Thailand

ARTICLE INFO

Keywords:
MG-63
Osteoblast-like cells
Osteosarcoma
Human mesenchymal stem cells
Bone matrix
Calcium nodules
Contact-inhibition
Nanostructure

ABSTRACT

Osteoblast-like cells and human mesenchymal stem cells (hMSCs) are frequently employed as osteoprogenitor cell models for evaluating novel biomaterials in bone healing and tissue engineering. In this study, the characterization of UE7T-13 hMSCs and MG-63 human osteoblast-like cells was examined. Both cells can undergo osteogenesis and produce calcium extracellular matrix; however, calcium nodules produced by MG-63 lacked a central mass and appeared flatter than UE7T-13. The absence of growing calcium nodules in MG-63 was discovered by SEM-EDX to be associated with the formation of alternating layers of cells and calcium extracellular matrix. The nanostructure and composition analysis showed that UE7T-13 had a finer nanostructure of calcium nodules with a higher calcium/phosphate ratio than MG-63. Both cells expressed high intrinsic levels of collagen type I alpha 1 chain, while only UE7T-13 expressed high levels of alkaline phosphatase, biomineralization associated (*ALPL*). High ALP activity in UE7T-13 was not further enhanced by osteogenic induction, but in MG-63, low intrinsic ALP activity was greatly induced by osteogenic induction. These findings highlight the differences between the two immortal osteoprogenitor cell lines, along with some technical notes that should be considered while selecting and interpreting the pertinent *in vitro* model.

1. Introduction

Bone is a dynamic, specialized connective tissue that responds continuously to hormonal, nutritional, and mechanical signals. When a bone is damaged, it has the ability to heal itself and regain function through a complex integration of cells, growth factors, and the extracellular matrix. Bone strength varies depending on the loading conditions. Under low-load conditions, such as when an astronaut is in zero gravity, osteoporosis can occur. Increased load, such as in the sports arm, boosts bone mass and strength. All of these dynamic changes are mediated by bone cells, specifically osteoblasts and their progenitor cells, mesenchymal stem cells (MSCs), preosteoblasts, and also osteoclasts, the bone resorbing cells.

In vitro culture of cells derived from bone has been investigated since 1964 [1]. Bone-derived cells, bone marrow stromal cells,

* Corresponding author.
E-mail address: charoenpanich_a@su.ac.th (A. Charoenpanich).

https://doi.org/10.1016/j.heliyon.2023.e15556
Received 3 October 2022; Received in revised form 7 April 2023; Accepted 13 April 2023
Available online 17 April 2023

trabecular bone derived cells, multipotential mesenchymal progenitor cells, osteoblast-like cells, osteoblastic cells, and primary osteoblasts are the terms frequently used to describe cells derived from bone, depending on their sources and identified characteristics. Originally, cells isolated from normal trabecular bone tissue (TB) obtained via collagenase treatment or bone explant were referred to as human osteoblast-like cells or primary osteoblasts, whereas adhesion cells isolated from bone marrow (BM) were referred to as bone marrow stromal cells [2,3]. However, it was discovered that both TB and BM-derived cells had identical epitopes that were positive for mesenchymal stem cell markers and negative for hematopoietic precursor cell markers [4]. Additionally, following 14 days of *in vitro* culture, the gene expression profiles of passage 0 TB-derived cells, which had previously diverged from BM-derived cells at day 0, became identical to those of BM-derived cells [4]. Moreover, both TB and BM-derived cells share the same fibroblastic appearance and the multilineage potential of bone, cartilage, and adipose tissues [5–9]. These TB and BM-derived multipotent cells are classified as human MSCs (hMSCs) [10].

The hMSCs are defined by their ability to adhere to plastic, their expression of surface markers (CD105(+), CD73(+), and CD90(+), and their multipotent properties [11]. The source of hMSCs is not restricted to bone tissue but can also be obtained from adipose tissue, placenta, cord blood, and dental pulp [12]. Since the release of the European Directive 2003/63/EC, hMSCs have been classified as advanced therapy medicinal products (ATMPs), and many researchers are seeking to establish hMSC culture protocols that meet good manufacturing practices [13–15]. Moreover, while hMSCs may be obtained noninvasively or from medical waste, their application in research is limited due to differences in cell morphology and features associated with donor age, donor-to-donor variation, and changes in cell morphology and characteristics associated with culture aging [16–18].

Human telomerase (hTERT) can be utilized to extend the lifespan of cells without causing genetic instability [19]. Various immortalized nontumorigenic hMSC lines had been generated and established as a research model via ectopic expression of human telomerase or a proto-oncogene while preserving the self-renewing and multilineage capacity of hMSCs [20–22]. UE7T-13 is one of the immortalized nontumorigenic hMSCs derived from bone marrow by infection with a retrovirus expressing human papillomavirus E7 and hTERT [23]. It has been demonstrated that UE7T-13 maintained the expression of hMSCs markers such as CD44, CD73, CD90, and CD105, as well as the multipotent capacity for osteogenic, adipogenic, chondrogenic, hepatogenic, and cardiac differentiation [24–28].

Furthermore, referred to as "osteoblast-like cells," are also osteosarcoma-derived cells exhibiting osteoblastic characteristics, such as the Saos-2 and MG-63 cell lines. Osteosarcoma derived osteoblast-like cells have been extensively employed in assessing the cytocompatibility of novel biomaterials and bone-induced regeneration agents [29]. These osteoblast-like immortal cell lines were preferred over primary cell culture in many studies due to various constraints such as a time-consuming isolation technique, limited cell numbers, a short life span, morphological and genetic instability, and donor-dependent response [30]. However, as their source was cancerous tissue, some of their tumorigenic characteristics may interfere with their responses, especially the invasion ability, including cell adhesion and growth [31–33].

A comparison of human bone marrow derived MSCs, and the MG-63 cells revealed that these cells share many characteristics [34]. The study demonstrated that hMSCs were composed of two unique populations of rapid self-renewal cells and flat cells (FC), with MG-63 being more similar to FC in terms of cell topography and morphological alterations when cultivated on different substrates. Furthermore, another study examined the biological responses of hMSCs, and the osteoblast-like cell lines MG-63, Saos-2, HOS, and U2OS to bioactive glass. This study indicated that MG-63 was most comparable to hMSCs, and suggested the use of MG-63 to evaluate bioactive glass and avoid donor-dependent variations [30]. In addition, MG-63 also expressed hMSC markers CD44 and CD90 [35], and was a very stable cell line that kept its phenotypic, adhesion receptors, cell cycle, and signaling proteins across all stages from passage 5 to passage 30 [36].

Furthermore, as reported in the literature, the MG-63 cell line is particularly interesting due to its stable phenotype and resemblance to hMSCs. This feature has made MG-63 cells a popular choice for testing the biocompatibility of biomaterials for orthopedic applications and investigating bone metabolism as an osteoblast-like cell [37–40]. Additionally, the MG-63 cell line has been used as an osteosarcoma model in bone cancer research, as it is derived from osteosarcoma and retains some cancer-like properties [41,42]. However, its tumorigenic property was usually neglected in the biomaterial characterization by avoiding the osteosarcoma term and calling as "osteoblast-like" cells. It is intriguing whether the tumorigenic cells could be a good representative cell line of osteoblast-like cells.

This study compared tumorigenic bone-derived cells (MG-63) with non-tumorigenic immortalized bone-derived human MSCs (UE7T-13) in terms of their growth, morphology, gene expressions, and bone matrix formation. The aim was to gain a better understanding of the similarities and differences between these cells, with potential implications for their use in bone tissue engineering. By highlighting these factors, caution can be exercised when utilizing these cells as *in vitro* models of bone-derived cells.

2. Method

2.1. Cell culture

Osteosarcoma cell line, MG-63 was purchased from the American Type Culture Collection, Rockville, MD, USA, Cat. No. 86051601; and human bone marrow-derived MSCs, UE7T-13, were purchased from the Japanese Collection of Research Bioresources Cell Bank (JCRB), Tokyo, Japan, Cat. No. JCRB1154. Both cell lines were maintained at 37 °C in a 5% carbon dioxide environment in complete growth media (CGM) with alpha modified Eagle's medium (α-MEM) (Hyclone, USA) supplemented with 10% fetal bovine serum (FBS) (Hyclone, USA), 100 μg/mL penicillin/streptomycin, and 2 mM L-glutamine (Corning®, USA).

2.2. Cell morphology and proliferation assay

In this assay, a low initial cell seeding density of 2,000 cells per well in 48-well plates was employed to allow for the observation of changes in cell morphology and growth over time. Cells were grown in CGM to enable cell attachment for 48 h. The cells were then grown for an additional 14 days. The resazurin assay was used to determine cell viability [43]. The cells were treated with 44 μM resazurin (Cat. No. 199303, Sigma-Aldrich) at selected time points for 3 h. The absorbances at 570 and 600 nm were determined using a microplate reader (VICTOR Nivo™). As previously indicated, the percent reduction of resazurin was determined [44,45]. Pictures were obtained to monitor changes in cell morphology every two days.

2.3. Adipogenic differentiation

UE7T-13 and MG-63 were seeded in 96-well plates at 5,000 cells per well. After 72 h, the media were changed to adipogenic differentiation media (ADM) containing α-MEM supplemented with 10% FBS, 2 mM L-glutamine, 100 μg/mL penicillin/streptomycin, 1 μM dexamethasone (Sigma, USA, Cat. No. D8893-1 MG), 10 μg/mL h-Insulin (Sigma, USA, Cat. No. I9278-5 ML), 100 μM indomethacin (Sigma, USA, Cat. No. I7378-5G), and 500 μM isobutylmethylxanthine (Sigma, USA, Cat. No. I5879-1G). The cells were fixed for 10 min in 4% paraformaldehyde, rinsed twice with phosphate-buffered saline (PBS), and stained for 10 min with oil red O solution (Sigma, USA, Cat. No. O1391) before being washed with distilled water prior to microscopic imaging after 21 or 28 days in ADM. Further, the cells were washed with PBS and fixed with 4% paraformaldehyde at room temperature for 15 min for BODIPY/DAPI fluorescence labeling. Briefly, Triton X-100 (0.1% in PBS, v/v) was used for 15 min to permeabilize cells, and staining with 10 μg/mL BODIPY 493/503 (Sigma, USA, Cat No. 121207-31) for 10 min was performed. The nuclei were counterstained with 1 μg/mL DAPI (Sigma, USA, Cat. No. 28718-90-3) for 5 min. Lipid droplets and nuclei were visualized under an inverted fluorescence microscope (Olympus, CKX53, Japan). The size distribution of lipid droplets was analyzed using ImageJ software, with at least 100 droplets analyzed per image from triplicates.

2.4. Osteogenic differentiation

MG-63 and UE7T-13 were cultured at 10,000 cells per well in a 48-well plate in CGM for 72 h prior to osteogenic induction in osteogenic differentiation medium (ODM). The ODM was composed of α-MEM and supplemented with 0.1 μM dexamethasone, 50 μM L-ascorbic acid (Sigma, USA, Cat. No. 50-81-7), and 10 mM β-glycerolphosphate disodium salt hydrate (Sigma, USA, Cat. No. G5422-25G). Cells were induced simultaneously and collected at the relevant time points.

Alizarin red staining was used to examine calcium nodules formed by the cells [46,47]. Cells were fixed with 70% ethanol for 30 min and then stained with 2% (w/v) Alizarin red, pH 4.1 (Sigma, USA, Cat. No. 130-22-3) for 15 min. The excess dye was rinsed with PBS three times before imaging. Images were taken under a stereo microscope and an inverted microscope. Acetic acid (10% v/v) was added to dissolve the stained calcium for quantification. The cells were scraped and heated at 85 °C for 10 min. Later, the cell suspension was incubated on ice for 5 min, and the supernatant was transferred to a fresh tube. The pH was adjusted to 4.5 using 10% ammonium hydroxide. The absorbance was recorded at 405 nm.

Total calcium deposits were quantified using a calcium liquid colorimetric assay [48,49]. Calcium was dissolved by overnight refrigeration at 4 °C shaking in 0.5 M hydrochloric acid (HCl) after 9, 15, or 21 days of osteogenic induction. The cells were scraped and transferred into a fresh 1.5 mL tube and centrifuged at 13,500 rpm for 5 min to remove cell debris. The supernatant was diluted at a 1:4 ratio in 0.5 M HCl, and 10 μL of the diluted sample was reacted with 190 μL of *o*-cresolphthalein complexone chromogenic agent. The absorbances were recorded at a wavelength of 570 nm. The regression line equation for the calcium calibration curve was used to determine the calcium content.

2.5. Gene expression analysis

Cells were grown at a density of 10,000 cells per well in a 48-well plate and cultured in CGM or ODM for the indicated time. Total mRNA was isolated using the RNA purification mini kit (Favorgen, Cat. No. FATRK001-1). The RNA yield was determined using NanoDrop™2000/2000c spectrophotometers (ThermoFisher Scientific). The names and sequences of primers are listed in supplementary Table S1. cDNA synthesis was carried out in accordance with the manufacturer's protocol using an RT-PCR master mix (containing Oligo dT) (GeneAll, Cat. No. 601–730). qRT-PCR was performed on a 7500 Fast Real-Time PCR System (Applied Biosystems™) and 2× iTaq™ Universal SYBR® Green Supermix (Biorad, Cat. No. 172–5122) was used. The PCR experiment was performed in triplicates. The amplification plot cycles were then followed by a melting curve analysis. The specificity of each PCR product was confirmed by a peak at the predicted melting temperature. The $2_{T}^{-\Delta\Delta C}$ method was used to calculate fold changes with GAPDH normalization at a cutoff value of two-fold change ($p < 0.05$).

2.6. Alkaline phosphatase staining

Alkaline phosphatase (ALP) is a marker for the development of bone tissue. The cell fixation with 70% ethanol for 30 min was followed by cell staining with a 0.2% (v/v) NBT/BCIP solution (Sigma-Aldrich, Cat. No. 11681451001) for 90 min prior to imaging [46,50]. BCIP is converted to a blue intermediate by alkaline phosphatase. NBT is subsequently used to oxidize the intermediate, resulting in the formation of an insoluble purple dye.

2.7. Scanning electron microscope (SEM) and energy dispersive X-ray spectroscopy (EDX) analysis

Cells were cultured on the 13 mm cover slip in a 24-well plate at 20,000 cells per well to prepare cells for SEM and EDX analysis. At the selected time point, cells were fixed with 2.5% (v/v) glutaraldehyde (Sigma-Aldrich, Cat. No. 111-30-8), pH 6–7 in a 0.1 M phosphate buffer for 1 h, followed by serial alcohol dehydration. Furthermore, prior to gold coating, critical point drying was accomplished using hexamethyldisilazane (HMDS) (Sigma-Aldrich, Cat. No. 999-97-3) [51]. The SEM and EDX were performed using the TESCAN Mira3 FE-SEM equipped with energy dispersive X-ray (Czech Republic). The average size of extracellular matrix (ECM) nanostructures was determined by examining SEM pictures from 10 distinct regions (n = 10) for each cell type using ImageJ.

2.8. Statistical analysis

All the experiments were conducted in triplicates (n = 3), unless stated otherwise. Statistical analysis was performed with the Statistical Package for the Social Sciences version 26.0 with an independent sample *t*-test. The p-values less than 0.05 were considered statistically significant ($*p < 0.05$).

3. Results

3.1. Cell morphology and growth rate

Microscopic imaging and resazurin-based assays were performed every two days for 14 days to determine changes in cell shape and cell proliferation. UE7T-13 and MG-63 exhibited a similar morphology with elongate rectangular or polygonal shapes for the first four days before confluence (Fig. 1a). Further, the cells reached the whole surface area of the culture vessels from day 6 on, and their morphology underwent distinct alterations. UE7T-13 assumed a long spindle shape and aligned with each other, whereas MG-63

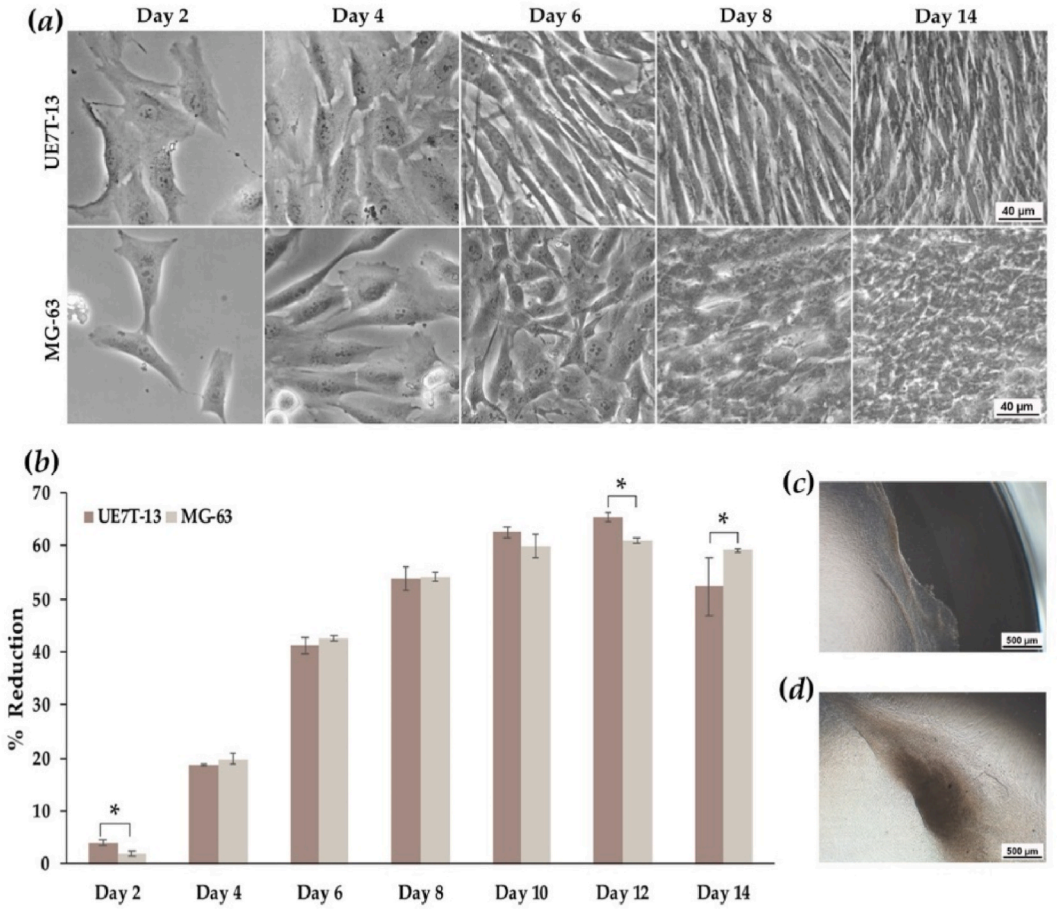

Fig. 1. Distinct morphological changes with comparable growth rates of UE7T-13 and MG-63. Cell morphology of UE7T-13 and MG-63 during their 14 days proliferation (*a*). The percentage reduction of resazurin was normalized to day 0 (*b*). Over-confluence UE7T-13 on day 14, resulting in cell sheet peel (*c*) or cell clumps around the well edge (*d*). $*p < 0.05$.

retained its original shape (Fig. 1a).

UE7T-13 showed the percentage reduction of resazurin normalized to day 0 was slightly greater at days 2 and 12 than in MG-63 (Fig. 1b). In addition, UE7T-13 and MG-63 grew at comparable rates when growth patterns and rates were compared (Fig. 1b). The growth rates of both cells were the highest between days 2 and 6, increasing by about 10% every day. After day 6, growth rates decreased to approximately 3–5% per day and reached a plateau after day 10. At day 14, a drop in the metabolic activity of UE7T-13 was observed. This could be the consequence of the cell sheet peeling off (Fig. 1c) or clumping together around the well edge (Fig. 1d).

3.2. Adipogenic differentiation

UE7T-13 and MG-63 cells were induced with adipogenic induction media. Both cells were capable of undergoing adipogenic differentiation and accumulating lipid droplets (Fig. 2). Large lipid droplets were visible along with a substantial amount of small lipid droplets in UE7T-13 after 21 days (Fig. 2a), whereas MG-63 formed a cluster of extremely small droplets (Fig. 2d). Clusters of lipid droplets were more apparent in both cell lines on day 28, with MG-63 maintaining clusters of small droplets (Fig. 2e and f) and UE7T-13 displaying clusters of both large and small droplets (Fig. 2b and c).

The scatter plot of lipid droplet size distribution revealed greater variance in UE7T-13, with droplet sizes ranging from less than 1 μm to approximately 8 μm (Fig. 2g). The majority of the MG-63 lipid droplets measured between 1 and 1.5 μm according to a histogram analysis (Fig. 2h).

3.3. Osteogenic differentiation

UE7T-13 and MG-63 were chemically induced in ODM for 21 days. Calcium deposition was visualized and quantified. On day 7, tiny calcium nodules with a homogenous distribution were observed in UE7T-13 (Fig. 3a). Further, accreted calcium was not visible in

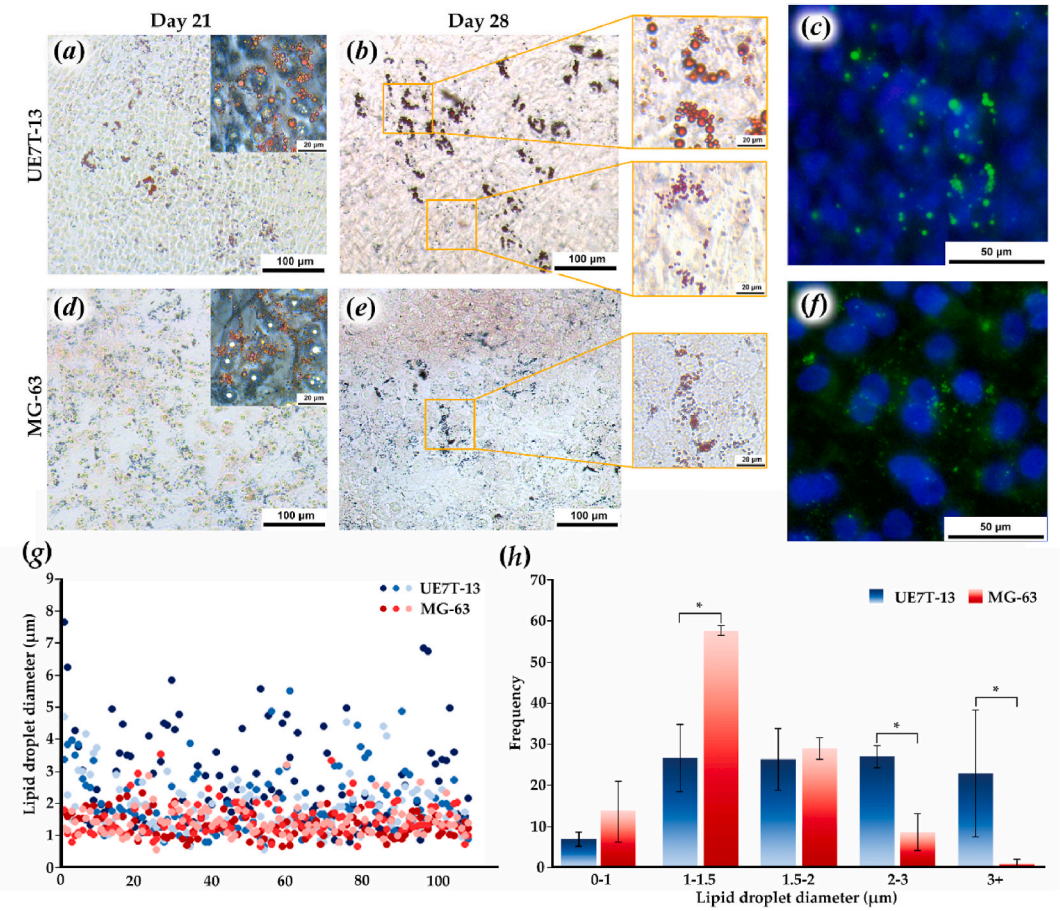

Fig. 2. Adipogenic differentiation of UE7T-13 (*a–c*) and MG-63 (*d–f*). Oil red O staining of lipid droplets after 21 days (*a, d*) and 28 days (*b, e*). The insets highlighted the size of stained lipid droplets under high magnification. Fluorescent images of lipid droplets stained with BODIPY 493/503 (green) and nuclear counterstaining with DAPI (blue) in UE7T-13 (*c*) and MG-63 cells (*f*) 28 days after adipogenic induction. The scatter plot (*g*) and histogram (*h*) of lipid droplet size distribution.

MG-63 without staining until day 9, when it developed as a small crystal that required greater magnification to observe (Fig. 3a and b). The calcium nodule in UE7T-13 was thicker and more nodule-like than the calcium nodule in MG-63, as evidenced by a darker appearance with a distinct boundary (Fig. 3a and b). Lack of nodule like structure of calcium ECM in MG-63 continued even in a prolonged culture of 45 days (Figure S1).

A calcium colorimetric assay was performed for the quantification of calcium deposition. At days 9, 15, and 21, UE7T-13 calcium deposition was substantially greater than that of MG-63 by 59.53%, 38.49%, and 25.42%, respectively (Fig. 3b).

Moreover, after 21 days, alizarin red staining confirmed the variations in calcium deposition between the two cell lines. Despite the staining area being comparable, UE7T-13 exhibited a considerably thicker calcium nodule than MG-63 (Fig. 3c). Furthermore, by dissolving the labeled calcium and measuring the absorbance at 405 nm on days 9, 12, and 14, revealed that UE7T-13 deposited over 100% more calcium than MG-63, with increases of 148.76%, 151.50%, and 118.58%, respectively (Fig. 3c). The difference was largest on day 12 and decreased on days 18 and 21–93.56% and 65.68%, respectively. Interestingly, the proportion of differences was significantly higher with alizarin red staining (Fig. 3c) than with the colorimetric assay (Fig. 3b).

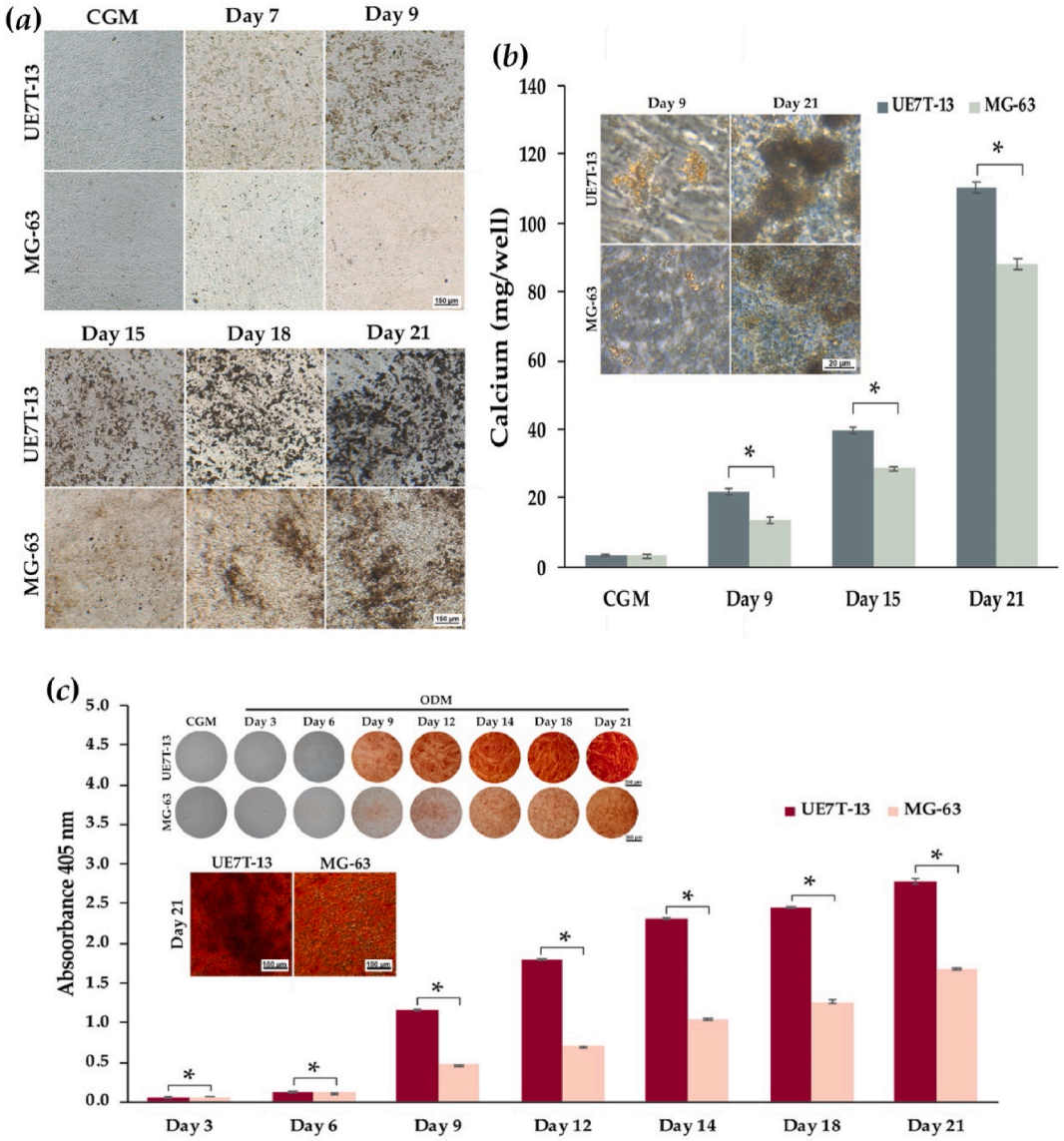

Fig. 3. Calcium deposition analysis. Microscopic images of calcium deposition by UE7T-13 and MG-63 (*a*). Quantitative analysis of accreted calcium and the insets of calcium nodules at high magnification (*b*). Images of alizarin staining (insets) and quantitative analysis of labeled calcium (*c*). *$p < 0.05$.

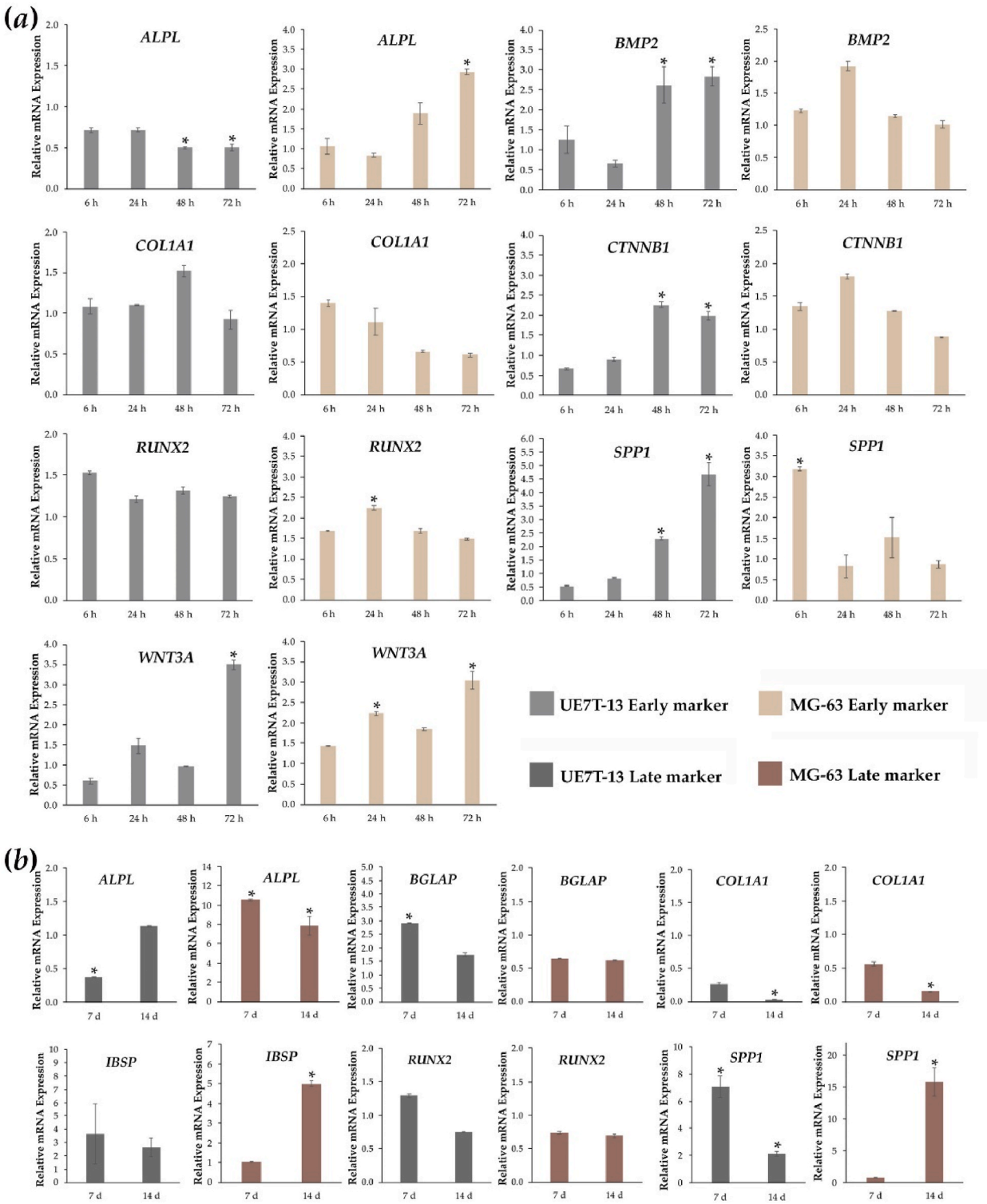

Fig. 4. Relative gene expression of bone markers in UE7T-13 and MG-63 during osteogenic induction. Data normalized to the gene expression of cells grown in CGM: UE7T-13 and MG-63 at early time points (*a*) and late time points (*b*). *$p < 0.05$ with a 2-fold cutoff.

3.4. Osteogenic marker gene expressions

qRT-PCR was used to evaluate the expression of established bone marker genes at multiple time points to monitor changes in gene expression profiles following osteogenic induction. Both cells can differentiate into osteoblasts and deposit mineralized ECM; however, their gene expression profiles were noticeably dissimilar.

In UE7T-13, osteogenic stimulation significantly upregulated the expression of *BMP2* and *CTNNB1* at 48 and 72 h, *SPP1* expression at 48 and 72 h, and *WNT3A* at 72 h, while *COL1A1* and *RUNX2* expression remained unaltered (Fig. 4a). Moreover, *ALPL* expression levels decreased at 48 and 72 h. Additionally, it was observed that osteogenic induction in UE7T-13 had no effect on any of the indicated markers at 6 or 24 h (Fig. 4a). In MG-63, *SPP1* was elevated by osteogenic induction at 6 h, and *RUNX2* expression was enhanced at 24 h, while *WNT3A* expression was increased at 24 and 72 h, and *ALPL* at 72 h (Fig. 4a). *BMP2*, *COL1A1,* and *CTNNB1* expressions were unaffected (Fig. 4a).

Six genes were analyzed at days 7 and 14: *ALPL, BGLAP, COL1A1*, *IBSP, RUNX2,* and *SPP1*. The results demonstrated that osteogenic induction significantly reduced *COL1A1* expression at day 14 in both cell lines (Fig. 4b). In UE7T-13, ODM suppressed *ALPL* expression at day 7 while stimulating the expression of *BGLAP* at day 7 and *SPP1* at days 7 and 14 (Fig. 4b). *ALPL* expressions were still substantially induced by ODM in MG-63, with 10.55- and 7.89-fold increases at days 7 and 14, respectively. At day 14, *SPP1* and *IBSP* expressions were both elevated in MG-63, with 15.72- and 5.02-fold increases, respectively (Fig. 4b).

Furthermore, to emphasize fundamental variations in gene expression, data were also presented as ΔC_T to avoid masking background expression using fold change normalization (Table 1). The ΔC_T values were averaged over four-time intervals from cells cultivated in CGM for 6, 24, 48, and 72 h (Table 1). *COL1A1* was the most abundant mRNA expressed in both UE7T-13 and MG-63, with an average ΔC_T value of 1.93 and 3.11 cycles, respectively (Table 1). In UE7T-13, *RUNX2* and *ALPL* were also highly expressed with an average ΔC_T of 6.08 and 7.70, respectively. *BMP2* and *CTNNB1* were the second and third most abundant transcripts in MG-63, with average ΔC_T values of 5.60 and 6.19, respectively. Highly expressed genes were not further induced in either cell line when data were arranged from the highest intrinsic expression (lowest ΔC_T value) to the lowest intrinsic expression, and, in some cases, such as *ALPL* in UE7T-13, they were reduced by osteogenic induction (Table 1).

3.5. Alkaline phosphatase activity

The results of the gene expression analysis showed that *ALPL,* a common marker of osteogenesis, was the most differently expressed gene between the two cell lines. While UE7T-13 expressed a high level of *ALPL* mRNA, osteogenic induction had little effect or lowered its expression (Fig. 4). *ALPL* mRNA expression was low in MG-63 during normal growth but was greatly increased by ODM (Fig. 4). ALP enzyme activity was then evaluated in both cell lines for 21 days after osteogenic induction using NBT/BCIP labeling.

The ALP staining results indicated that UE7T-13 possessed an intrinsically high level of ALP activity, as indicated by the presence of a strong purple stain in CGM conditions since day 3 (Fig. 5a). ALP activity increased in UE7T-13 until day 7 and remained elevated until day 21 without osteogenic induction. ODM had no positive effect on ALP activity, and the blue staining of ALP in ODM appeared to be diminished on days 10–18 (Fig. 5a).

The ALP activity in MG-63 was negligible throughout 21 days in CGM without osteogenic induction; however, on osteogenic induction, ALP activity increased gradually over time since day 5 (Fig. 5b). Furthermore, ALP activity appeared to be similar on days 7–14, but markedly increased on days 18 and 21 (Fig. 5b). The results were consistent with those obtained using qRT-PCR. This result established the distinct ALP functions in the two cell lines.

3.6. SEM-EDX analysis

The cell morphology and calcium nodule structure during the early stages of calcium deposition were analyzed using SEM analysis. On the basis of the appearance of calcium nodules and the similar amount of calcium, the samples were collected on day 9 for UE7T-13 and day 15 for MG-63 (Fig. 3a and b). Cell morphology was observed to be different between UE7T-13 and MG-63. UE7T-13 exhibited elongated spindle cells, while MG-63 exhibited shorter rectangular cells, similar to the result from phase-contrast light microscopy (Fig. 6a, 1a). Additionally, MG-63 produced a large number of small fibrils with a diameter of approximately 115.7 ± 21.4 nm (n = 10)

Table 1
Average ΔC_T values of early marker genes in UE7T-13 and MG-63 from 6, 24, 48, and 72 h and their changes in response to osteogenic induction. *Statistically significant; Ns: not significant.

Expression level	UE7T-13			MG-63		
	Gene	ΔC_T	ODM	Gene	ΔC_T	ODM
Highest	*COL1A1*	1.93 ± 2.41	Ns	*COL1A1*	3.11 ± 2.58	Ns
Lowest						
	RUNX2	6.08 ± 1.14	Ns	*BMP2*	5.60 ± 1.17	Ns
↓	*ALPL*	7.70 ± 0.20	Down*	*CTNNB1*	6.19 ± 2.32	Ns
	CTNNB1	8.23 ± 2.43	Up*	*RUNX2*	6.48 ± 2.42	Up*
↓	*SPP1*	11.31 ± 1.49	Up*	*WNT3A*	7.03 ± 1.46	Up*
	WNT3A	11.86 ± 0.82	Up*	*ALPL*	12.31 ± 0.62	Up*
Lowest	*BMP2*	12.97 ± 0.98	Up*	*SPP1*	14.97 ± 2.53	Up*

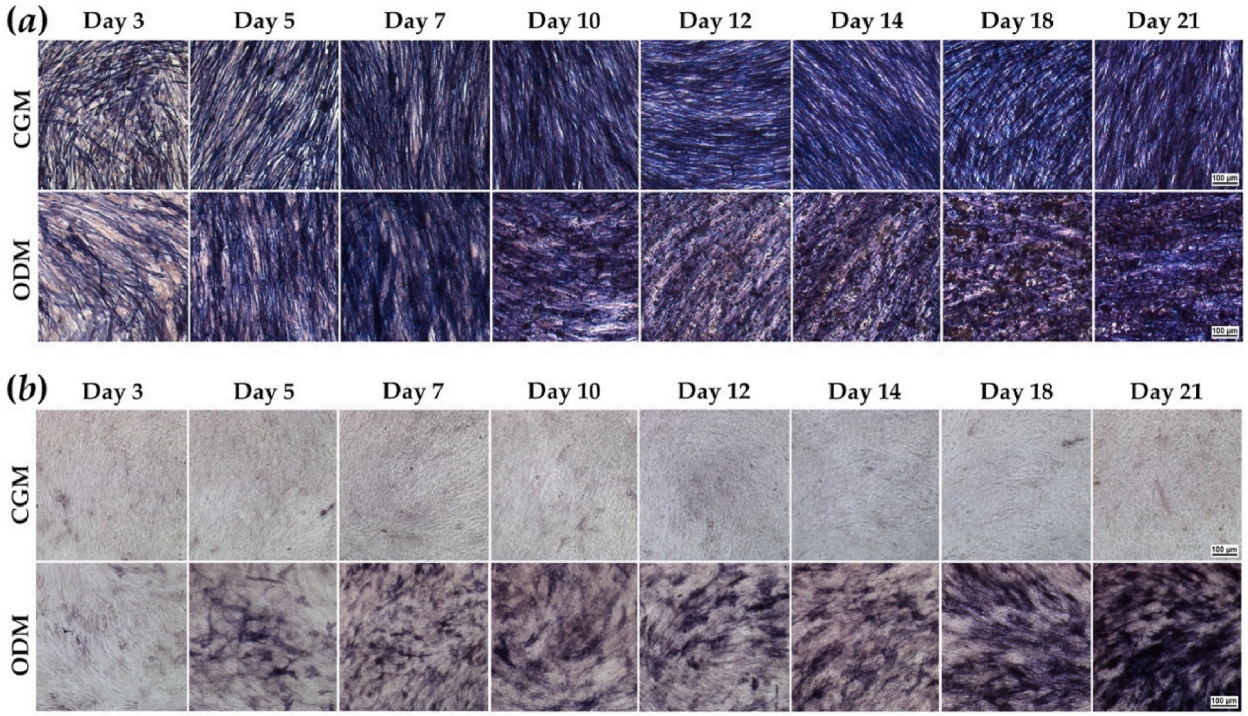

Fig. 5. ALP activity and its variations in response to osteogenic induction in UE7T-13 (*a*) and MG-63 (*b*).

(Fig. 6a).

Calcium nodules with a consistent distribution can be easily distinguished and differentiated from UE7T-13 at a magnification of 500× (Fig. 6b). Further, the SEM revealed that the calcium nodules in UE7-13 were laid on top of cells with a size larger than the cells at a 2 kx magnification, whereas the calcium nodule in MG-63 was not visible (Fig. 6b). MG-63 contained a relatively small number of mineralized ECM which were difficult to identify but can be observed at a magnification of 20 kx (Fig. 6b). Moreover, SEM-EDX analysis confirmed the presence of calcium phosphate in the selected area (area 1, Fig. 7a and b). Elemental composition analysis revealed that UE7T-13 had greater calcium-phosphate ratio than MG-63, with a ratio of 1.58 (2.04 by weight) as compared to 1.24 (1.60 by weight). Furthermore, another notable difference was the amount of nitrogen and oxygen. MG-63 had a higher nitrogen content, while UE7T-13 had a much higher oxygen content.

The nanostructure of the calcium nodule was viewed at 500 kx and 1000 kx (Fig. 7c–e). The nanostructure of the mineralized ECM was comparable between the two cell lines. Crystalline apatite was embedded within the collagenous extracellular matrix and appeared as a continuous line with considerable roughness visible on the surface as multiple edges. However, these nanostructures in MG-63 had an average diameter of approximately 202.0 ± 27.0 nm, which were significantly larger than the average diameter of calcium crystals in UE7T-13, which was about 117.8 ± 27.9 nm ($n = 10$, $p < 0.01$) (Fig. 7c–e).

The day 15 sample of MG-63 had relatively few calcium nodules (Fig. 7b), which did not correspond to the previous calcium quantification result (Fig. 3b). Hence, another sample of MG-63 from day 18 was examined. To our surprise, the obvious calcium nodules remained unnoticed (Fig. 8a). However, with further investigation, disparities between the MG-63 in ODM and CGM were discovered due to the presence of numerous bumping areas (Fig. 8a). Furthermore, back scatter electron (BSE) was then used to determine the atomic contrast of elements in the area. The BSE results revealed that the bumping region had elements with a higher atomic number than the surrounding area, as they appeared brighter than the surrounding area (Fig. 8b). Additionally, the EDX analysis confirmed a significant calcium and phosphorus content in the area (Fig. 8b).

Moreover, MG-63 cells grown in CGM formed a substantial amount of ECM on the cell surface, which resembled calcium nodules (Fig. 8c). The ECM nanostructure was smoother than that of ECM containing crystal apatite, according to enhanced magnification of 20 kx. EDX analysis verified that this ECM did not contain calcium and was predominantly composed of carbon, oxygen, and nitrogen (Fig. 8*c*).

The re-analysis of the day 15 sample of MG-63 with BSE revealed several bright spots, confirming the calcium mineralized area in the sample, which had been covered up (Fig. 9a). Moreover, MG-63 cells developed and expanded on top of calcium nodules. A fractured area (Fig. 9b) that exposed the calcium nodules beneath and a well-covered calcium area that was completely covered by cells in MG-63 day 15 sample were identified (Fig. 9c).

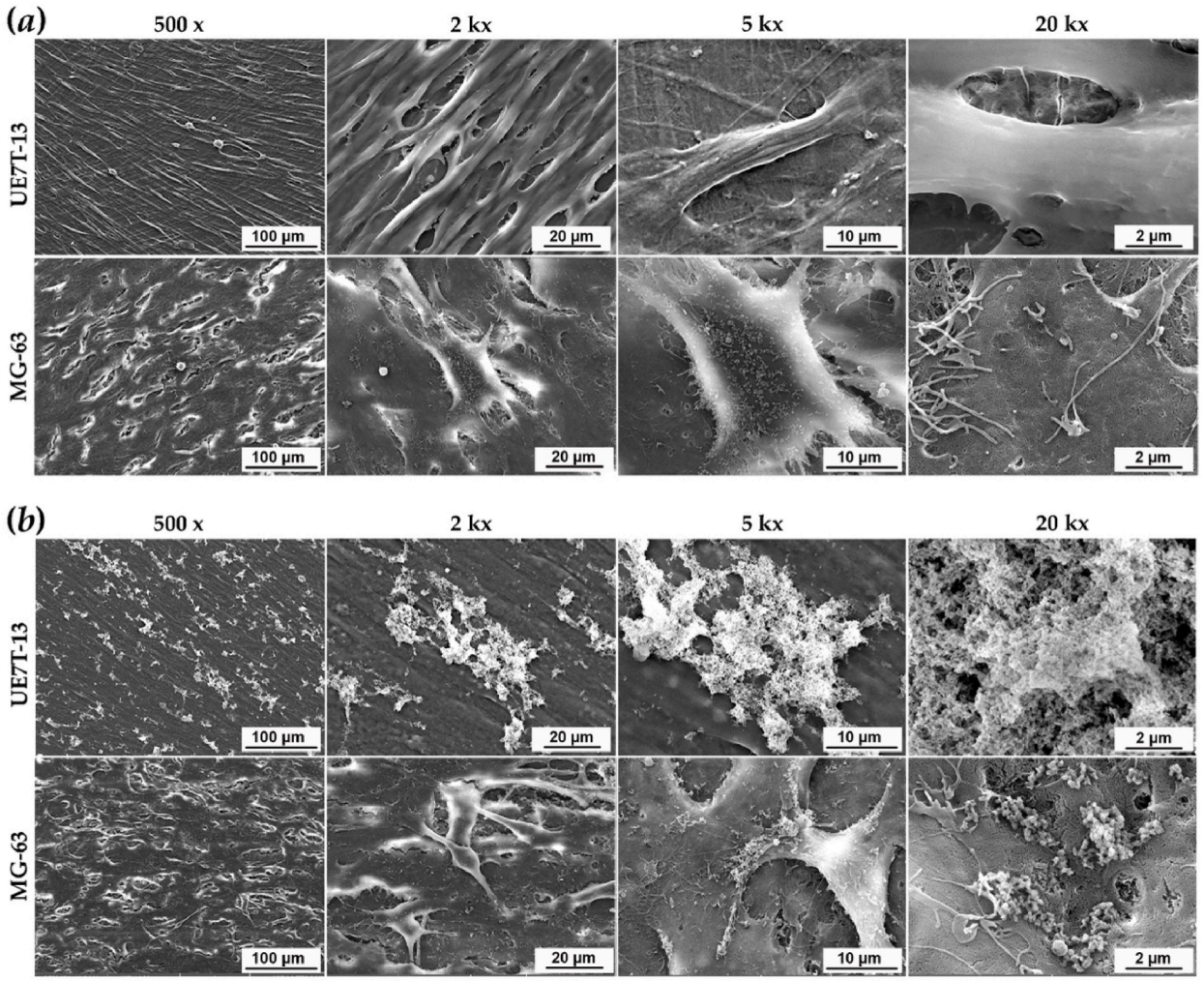

Fig. 6. Cell morphology and calcium nodule. Representative SEM images showed morphology of UE7T-13 at 9 days and MG-63 at 15 days in growth media (*a*) and calcium nodule formation of UE7T-13 at 9 days and MG-63 at 15 days in osteogenic induction media (*b*).

4. Discussions

In vitro cell culture models have been widely used to characterize potential biomaterials for bone regeneration and bone tissue engineering. The selection of appropriate cells is a vital step in advancing our understanding of physiological interaction and tissue regeneration in order to achieve the desired clinical outcome of implant materials. MSCs and osteoblast-like cells derived from osteosarcoma are two of the most commonly used human cells in bone biomaterial characterization. In this study, the hMSCs, UE7T-13, and osteoblast-like MG-63 cell lines were chosen, and their osteogenesis-related alterations were characterized, including morphological changes, temporal gene expression regulation, and formation of bone extracellular matrix.

The growth rate of MG-63 was comparable to that of UE7T-13. However, it lacked contact inhibition, maintained its morphology, and continued to grow on top of each other. MG-63 is one of the osteosarcoma cell lines generated from tumor in 1978 [52]. The majority of early human cell lines are cancellous cells that can be isolated and cultivated indefinitely. MG-63 has been suggested and employed as an osteoblastic phenotypic model due to its ability to secrete osteocalcin and alkaline phosphatase in response to 1, 25-(OH)2D3 and parathyroid hormone (PTH) treatment [53]. UE7T-13 is a human telomerase reverse transcriptase (TERT) and human papillomavirus E7 gene-expressing immortalized human mesenchymal stem cell (hMSC) line derived from bone marrow (hBMSC) [23]. Moreover, the lifespan of UE7T-13 was extended, its characteristics as a hMSC with multipotency were preserved [23,26]. In addition, it was shown in this study that UE7T-13 kept a hMSC phenotype and changed into elongated, parallel aligned cells after confluence.

The adipogenic and osteogenic differentiation of UE7T-13 and MG-63 cells were confirmed in this work. Adipogenesis in MG-63 was previously reported with similar ADM components [54]. Furthermore, MG-63 formed much smaller lipid droplets compared to UE7T-13 and with increasing the time of culture from 21 to 28 days did not changes this characteristic. BODIPY 493/503 was also

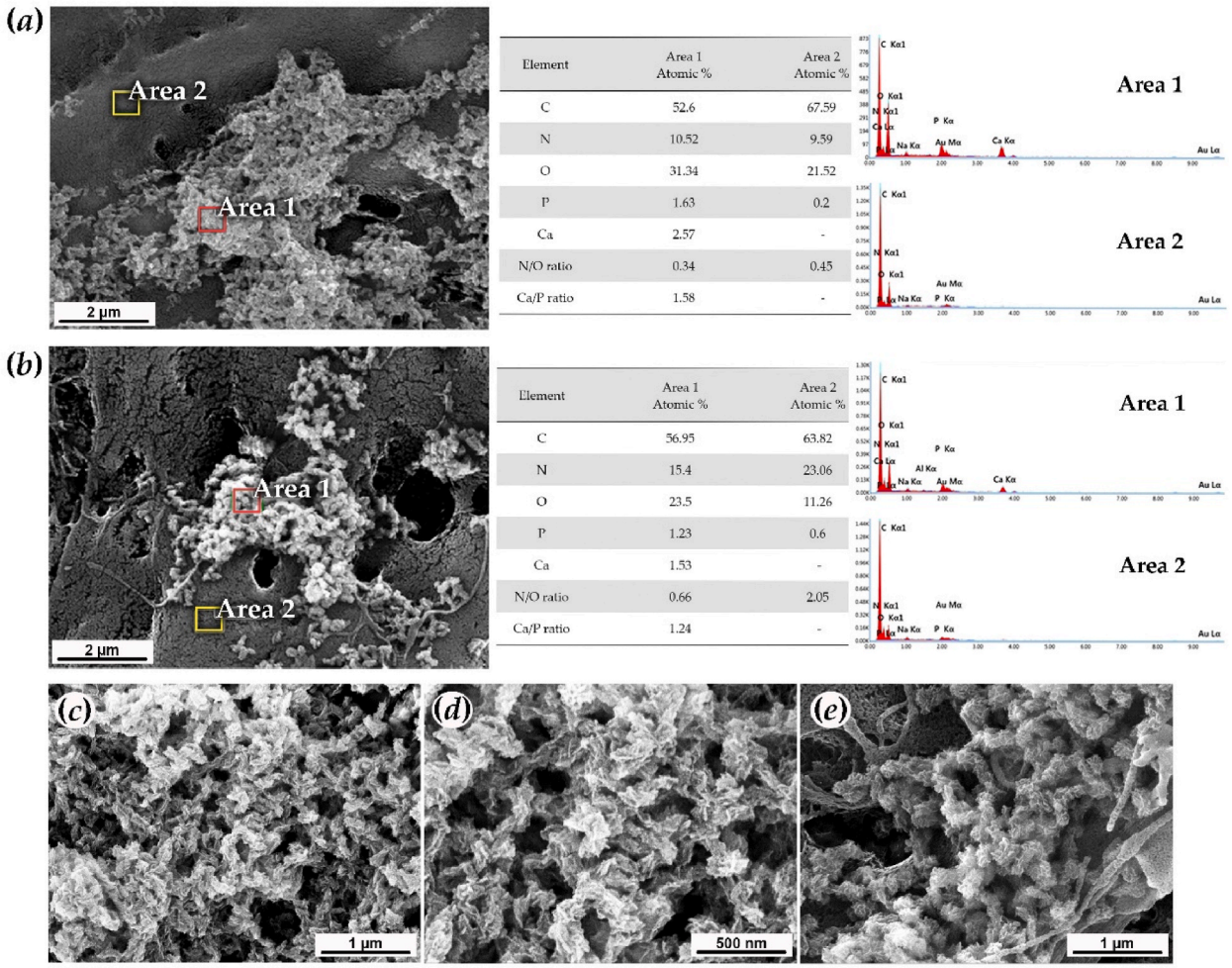

Fig. 7. SEM-EDX analysis of calcified ECM of UE7T-13 day 9 (*a*) and MG-63 day 15 (*b*) in ODM. Nanostructure of calcium nodule in UE7T-13 (*c, d*) and MG-63 (*e*).

used, and identical results were obtained, as previously stated that the alcohol fixative in oil red O staining may cause artifactual fusion of lipid droplets [55]. A cluster of tiny lipid droplets was also observed when MG-63 was induced to undergo adipogenesis with a dose of dexamethasone that was 10 times higher than the amount used in our investigation [56]. Increased lipid droplet size was associated with droplet fusion and a cascade of lipid droplet-lipid droplet contact, followed by the formation of a channel that mediates the transfer of neutral lipids between lipid droplets [57]. Compared to 2D culture, 3D spheroid culture enhanced the size of lipid droplets in canine osteosarcoma cell lines in conjunction with perilipins expressions [58]. The changes in lipid profiles of metastasizing osteosarcoma cells were identified in comparison with those of nonmetastatic cells [59]. The involvement of lipid metabolism and lipid droplets has been considered an essential cellular process of cancer capability, including tumorigenicity, invasion, metastasis, and chemoresistance [60]. Further investigation is required to discover whether the differences in lipid droplet formation between the two cell lines are associated with the tumorigenic properties or multilineage potential of MG-63.

Comparative examination of UE7T-13 and MG-63 alterations during their proliferation and osteogenic induction revealed significant discrepancies in their gene regulation as well as variances in the intrinsic expression of osteogenic marker genes. Both UE7T-13 and MG-63 exhibited substantial amounts of *COL1A1,* with or without osteogenic induction. Additionally, a prior study using RNAseq to assess the temporal expression of skeletally related genes in hBMSC-TERT showed that *COL1A1* maintained a constant expression level with a high abundance even in the absence of osteogenic induction at 0 h [61]. In this study, UE7T-13 highly expressed *RUNX2* and *ALPL* without additional osteogenic induction. According to a study on the origin of hMSCs, hMSCs produced from bone marrow expressed much more *ALPL* and *RUNX2* than hMSCs obtained from adipose tissue [62]. *RUNX2*, a master transcriptional regulator of osteoblastogenesis, was observed to correlate with a stronger osteogenic differentiation capacity of hBMSC than placental MSC [63]. *ALPL* expression was much lower in MG-63 than in UE7T-13 but was significantly increased in response to osteogenic stimulation. *ALPL* expression was similarly found to be low in MG-63 cells when compared to other bone-derived cells [29]. Additionally, less *ALPL* expression in MG-63 compared to primary bone explant cells was suggested to be a result of increased DNA methylation [64].

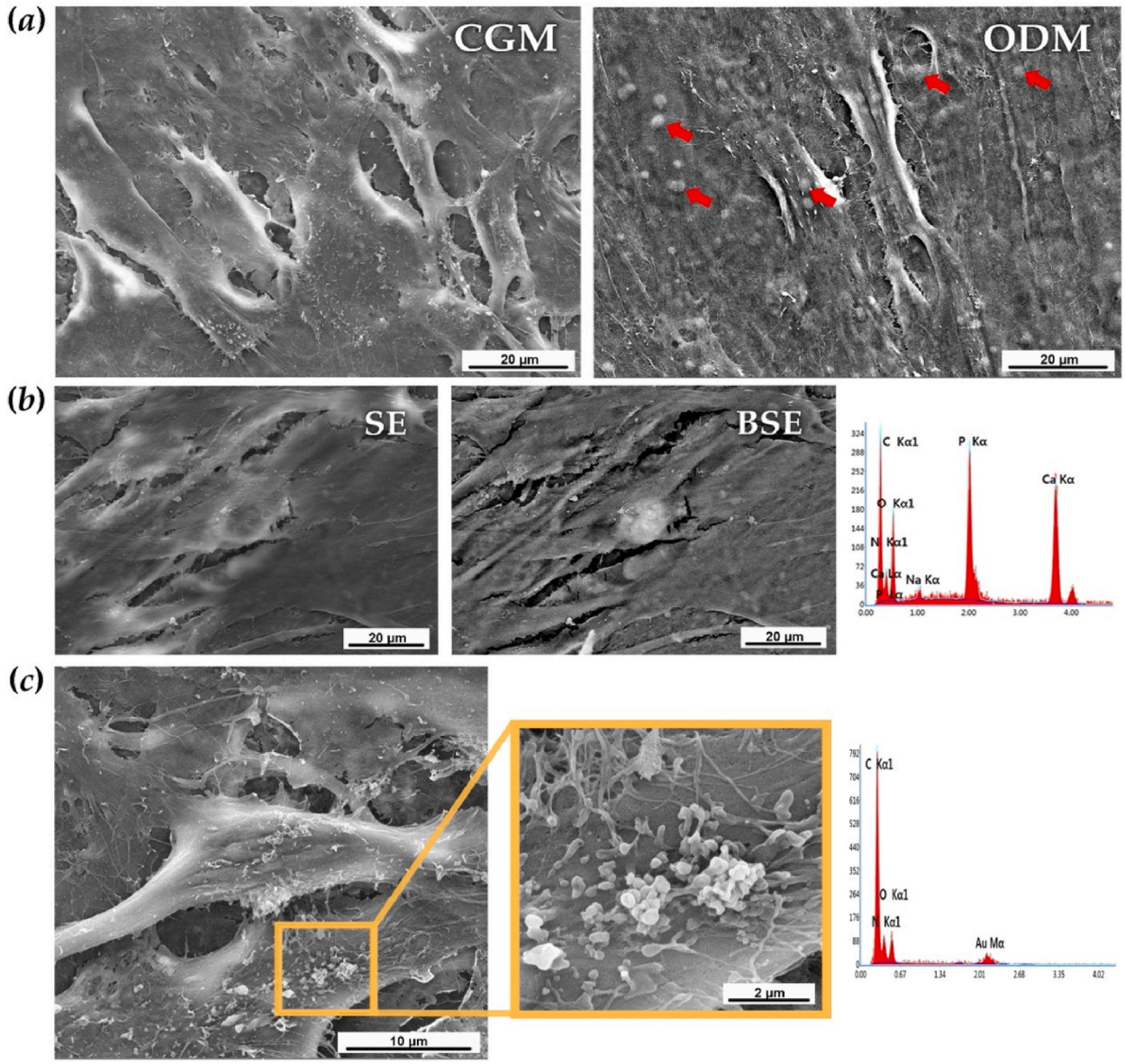

Fig. 8. SEM-EDX analysis of MG-63 **day 18**. Overview of the differences between cells in CGM and ODM (*a*). EDX analysis confirmed the presence of calcium in the bumping area of normal scanning electron (SE) mode with high atomic contrast when viewed in back scatter electron (BSE) mode (*b*). High magnification MG-63 day 18 in CGM showed the non-mineralized ECM that could be mistaken for calcium nodules at low magnification SEM (*c*).

In the current study, genes with a high baseline expression level, such as *COL1A1, RUNX2,* and *ALPL* in UE7T-13 and *COL1A1, BMP2, CTNNB1,* and *BGLAP* in MG-63, remained unaffected by osteogenic induction from ODM. After 48 h of osteogenic induction, *CTNNB1, SPP1*, and *BMP2* were elevated in UE7T-13. In MG-63, *SPP1* expression was increased as early as 6 h, followed by *RUNX2* and *WNT3A* expression at 24 h, and *ALPL* at 72 h. The canonical Wnt signaling pathway has been shown to induce osteogenesis by directly boosting *RUNX2* expression [65]. *In vitro*, direct addition of *WNT3A* to hMSCs stimulated ALP expression and activity [66]. With the high expression of *COL1A1* and *ALPL*, UE7T-13 looked to be closer to osteoprogenitor cells than multipotent stem cells, whereas MG-63 appeared to be more like mature osteoblasts with heavily expressed *BGLAP* [67].

Comparing calcium nodules in alizarin red staining results following osteogenic induction, UE7T-13 maintained the calcium nodule pattern of primary MSCs with discrete patches rather than large areas of dense mineralized structures. Calcium deposition in UE7T-13 developed quicker and was denser than in MG-63. In conjunction with the SEM-EDX results, the flatter appearance of calcium deposition in MG-63 may be due to its proliferation without contact inhibitions, which permits it to grow on top of the calcium layer and build multilayers of cells-alternative mineralized ECM. Previous research in U2OS cells, which are osteoblast-like cells derived

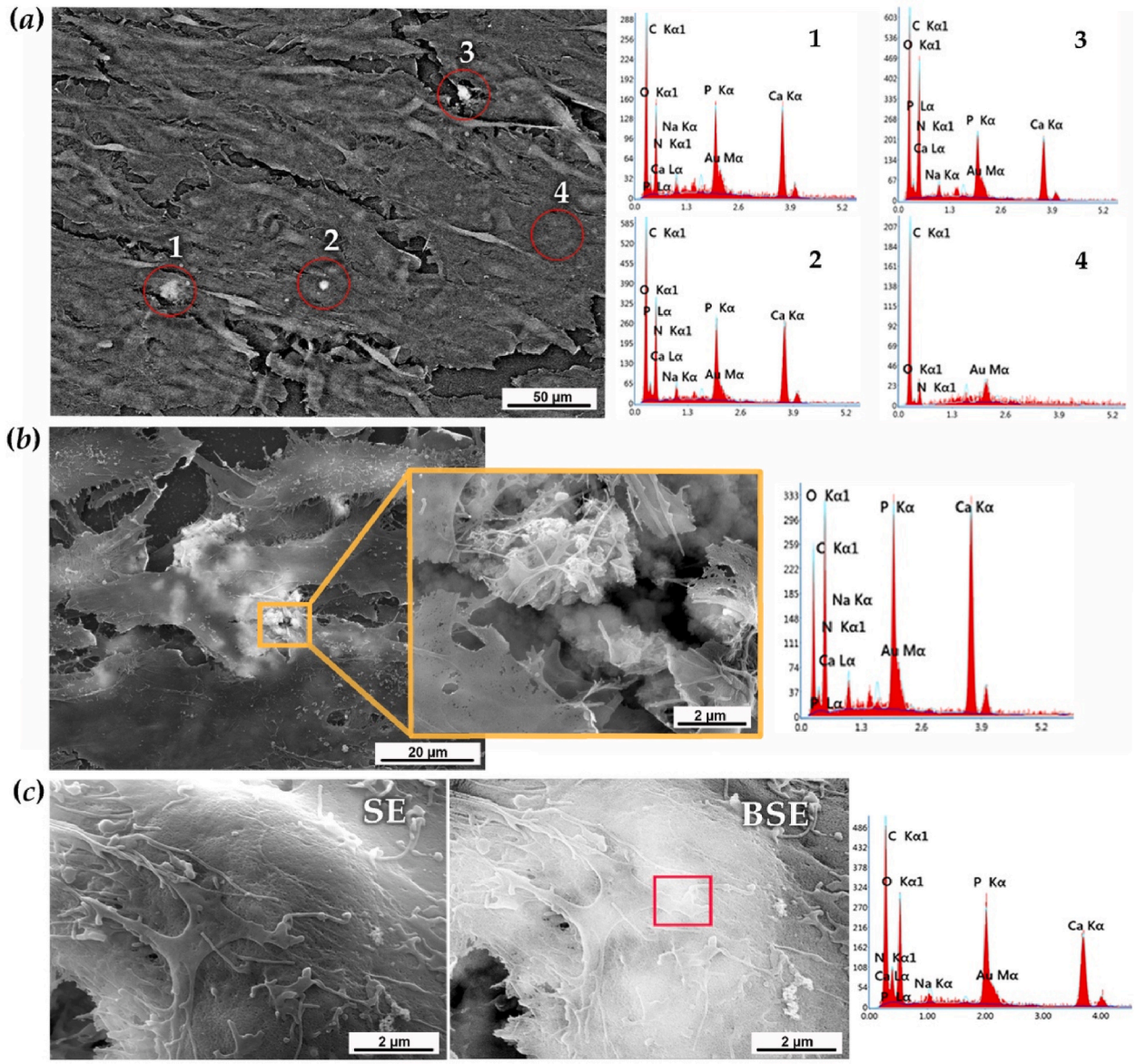

Fig. 9. SEM-EDX analysis of MG-63 **day 15 in ODM**. The atomic contrast image from back scatter electron (BSE) and EDX analysis revealed three bright spots (1–3) with high calcium and phosphate compared to the reference area (4) (*a*). Calcium nodules hidden underneath MG-63, with some exposed areas (*b*), and a well-covered area (*c*).

from osteosarcoma, revealed that U2OS cells produced mineralized ECM in dense multilayers [68]. The cells' alternative mineralized ECM in MG-63 may also hinder calcium detection. This led to an underestimation of calcium formation and a greater difference in calcium deposition between the two cell lines, as evaluated by alizarin red staining rather than calcium liquid color.

SEM-EDX analysis of the calcium nodule revealed a similar nanostructure between the two cell lines but differences in size and element composition. UE7T-13 had a greater CaP ratio than MG-63, with a weight ratio of 2.04, which is closer to the CaP ratio of 2.16 found in hydroxyapatite. CaP ratio in human bone can range from 2.1 to 2.6 depending on bone locations, and individual characteristics [69,70]. Additionally, the culture system can affect the calcium nodule's CaP ratio during *in vitro* osteogenesis [71]. It has been postulated that the hydroxyapatite/collagen ratio may be utilized as an indication of bone disorders, of which osteosarcoma had a greater amount of collagen, and the CaP ratio was higher in osteolytic osteosarcoma and lower in sclerotic osteosarcoma [72]. High nitrogen ratio in MG-63 may be indicative of increased ECM protein; however more investigation is necessary to determine the correlation between collagen and CaP ratio in the MG-63 calcium nodule.

Transplantation of human MSCs (hMSCs) has demonstrated benefits in the regeneration of various tissues, not limited to bone [73–76]. While the use of hMSCs in combination with other factors or gene therapy has the potential for anti-tumorgenicity [77,78],

other studies have demonstrated that hMSCs can promote tumor growth and metastasis *in vivo* [79,80]. However, there have been reports of low survival rates of hMSCs after implantation, attributed to their inability to adapt to metabolic activities *in vivo* [81]. Osteosarcoma-derived cells, such as the MG-63 xenograft model, are well-known models for *in vivo* tumor studies [82]. While MG-63 cells have been extensively used for biomaterial characterizations *in vitro*, their use in combination with scaffolds for *in vivo* transplants is usually avoided [83,84]. This study has demonstrated differences in morphological changes, proliferation patterns, lipid droplet formations, and bone matrix formation of the two bone-derived cell lines, MG-63 and UE7T-13, *in vitro*. However, it should be noted that cellular processes are complex and can be drastically altered by environmental changes. Therefore, further *in vivo* research is needed to confirm the findings and to understand the mechanisms underlying these differences.

5. Conclusion

This investigation revealed that the major difference between the two cell lines in terms of cell shape and matrix formation was mostly attributable to the malignant potential of MG-63, as shown by uninhibited expansion and the formation of calcium nodules that cover beneath the cells. With these characteristics, MG-63 might be more clinically relevant to that of osteosarcoma than as a model of osteoblast-like cells. Cautions should be used when utilizing MG-63 as an osteoblastic model, specifically when studying the development of extracellular matrix and morphological changes. Moreover, utilizing a human osteoprogenitor cell line, such as UE7T-13, during the early phases of therapeutic agent evaluation or for cytocompatibility testing may be a superior alternative for ensuring consistency in result comparisons, nontumorigenic, and the lack of interspecies variances.

Author contribution statement

Kamonwan Chatree; Patsawee Sriboonaied: Performed the experiments; Analyzed and interpreted the data. Wrote the paper.
Chinnatam Phetkong; Witoon Wattananit: Performed the experiments. Wrote the paper.
Chanpen Chanchao: Conceived and designed the experiments Wrote the paper.
Adisri Charoenpanich: Conceived and designed the experiments; Analyzed and interpreted the data; Contributed reagents, materials, analysis tools or data; Wrote the paper.

Funding statement

This work was supported by Development and Promotion of Science and Technology Talents Project (DPST), Institute for the Promotion of Teaching Science and Technology, Thailand {033/2558}.

Data availability statement

Data included in article/supplementary material/referenced in article.

Declaration of competing interest

The authors declare that they have no known competing financial interests or personal relationships that could have appeared to influence the work reported in this paper.

Appendix A. Supplementary data

Supplementary data related to this article can be found at https://doi.org/10.1016/j.heliyon.2023.e15556.

References

[1] W.A. Peck, S.J. Birge Jr., S.A. Fedak, Bone cells: biochemical and biological studies after enzymatic isolation, Science 146 (1964) 1476–1477.
[2] G.L. Wong, R.A. Luben, D.V. Cohn, 25-dihydroxycholecalciferol and parathormone: effects on isolated osteoclast-like and osteoblast-like cells, Science 197 (1977) 663–665.
[3] S.Y. Epikhina, N. Latsinik, Proliferative activity of clonogenic bone marrow stromal precursor cells, Bull. Exp. Biol. Med. 81 (1976) 67–69.
[4] Y. Sakaguchi, I. Sekiya, K. Yagishita, S. Ichinose, K. Shinomiya, T. Muneta, Suspended cells from trabecular bone by collagenase digestion become virtually identical to mesenchymal stem cells obtained from marrow aspirates, Blood 104 (2004) 2728–2735.
[5] S.H. Bernacki, M.E. Wall, E.G. Loboa, Isolation of human mesenchymal stem cells from bone and adipose tissue, Methods Cell Biol. 86 (2008) 257–278.
[6] U. Nöth, A.M. Osyczka, R. Tuli, N.J. Hickok, K.G. Danielson, R.S. Tuan, Multilineage mesenchymal differentiation potential of human trabecular bone-derived cells, J. Orthop. Res. 20 (2002) 1060–1069.
[7] R. Tuli, M.R. Seghatoleslami, S. Tuli, M.L. Wang, W.J. Hozack, P.A. Manner, K.G. Danielson, R.S. Tuan, A simple, high-yield method for obtaining multipotential mesenchymal progenitor cells from trabecular bone, Mol. Biotechnol. 23 (2003) 37–49, https://doi.org/10.1385/MB:23:1:37.
[8] K.B. Jonsson, A. Frost, O. Nilsson, S. Ljunghall, Ö. Ljunggren, Three isolation techniques for primary culture of human osteoblast-like cells: a comparison, Acta Orthop. Scand. 70 (1999) 365–373.
[9] V. Sottile, C. Halleux, F. Bassilana, H. Keller, K. Seuwen, Stem cell characteristics of human trabecular bone-derived cells, Bone 30 (2002) 699–704.

[10] L. Song, N.J. Young, N.E. Webb, R.S. Tuan, Origin and characterization of multipotential mesenchymal stem cells derived from adult human trabecular bone, Stem Cell. Dev. 14 (2005) 712–721.

[11] J. Steens, D. Klein, Current strategies to generate human mesenchymal stem cells in vitro, Stem Cell. Int. (2018), 6726185, https://doi.org/10.1155/2018/6726185.

[12] H. Klingemann, D. Matzilevich, J. Marchand, Mesenchymal stem cells–sources and clinical applications, Transfus. Med. Hemotherapy 35 (2008) 272–277.

[13] S. Bhat, P. Viswanathan, S. Chandanala, S.J. Prasanna, R.N. Seetharam, Expansion and characterization of bone marrow derived human mesenchymal stromal cells in serum-free conditions, Sci. Rep. 11 (2021) 1–18.

[14] S. Muthu, M. Jeyaraman, M.B. Kotner, N. Jeyaraman, R.L. Rajendran, S. Sharma, M. Khanna, S.N.S. Rajendran, J.M. Oh, P. Gangadaran, Evolution of mesenchymal stem cell therapy as an advanced therapeutic medicinal product (ATMP)—an Indian perspective, Bioengineering 9 (2022) 111.

[15] K. Kim, S. Bou-Ghannam, H. Thorp, D.W. Grainger, T. Okano, Human mesenchymal stem cell sheets in xeno-free media for possible allogenic applications, Sci. Rep. 9 (2019) 1–12.

[16] P. Ganguly, J.J. El-Jawhari, A.N. Burska, F. Ponchel, P.V. Giannoudis, E.A. Jones, The analysis of *in vivo* aging in human bone marrow mesenchymal stromal cells using colony-forming unit-fibroblast assay and the $CD45^{low}CD271^{+}$ phenotype, Stem Cell. Int. (2019), 5197983, https://doi.org/10.1155/2019/5197983.

[17] V. Ashapkin, V. Khavinson, G. Shilovsky, N. Linkova, B. Vanuyshin, Gene expression in human mesenchymal stem cell aging cultures: modulation by short peptides, Mol. Biol. Rep. 47 (2020) 4323–4329.

[18] Y.-H.K. Yang, C.R. Ogando, C. Wang See, T.-Y. Chang, G.A. Barabino, Changes in phenotype and differentiation potential of human mesenchymal stem cells aging in vitro, Stem Cell Res. Ther. 9 (2018) 1–14.

[19] M.M. Ouellette, L.D. McDaniel, W.E. Wright, J.W. Shay, R.A. Schultz, The establishment of telomerase-immortalized cell lines representing human chromosome instability syndromes, Hum. Mol. Genet. 9 (2000) 403–411, https://doi.org/10.1093/hmg/9.3.403.

[20] A. Nagai, W.K. Kim, H.J. Lee, H.S. Jeong, K.S. Kim, S.H. Hong, I.H. Park, S.U. Kim, Multilineage potential of stable human mesenchymal stem cell line derived from fetal marrow, PLoS One 2 (2007), e1272.

[21] B.M. Abdallah, M. Haack-Sørensen, J.S. Burns, B. Elsnab, F. Jakob, P. Hokland, M. Kassem, Maintenance of differentiation potential of human bone marrow mesenchymal stem cells immortalized by human telomerase reverse transcriptase gene despite of extensive proliferation, Biochem. Biophys. Res. Commun. 326 (2005) 527–538.

[22] M. Skårn, P. Noordhuis, M.-Y. Wang, M. Veuger, S.H. Kresse, E.V. Egeland, F. Micci, H.M. Namløs, A.-M. Håkelien, S.M. Olafsrud, Generation and characterization of an immortalized human mesenchymal stromal cell line, Stem Cell. Dev. 23 (2014) 2377–2389.

[23] T. Mori, T. Kiyono, H. Imabayashi, Y. Takeda, K. Tsuchiya, S. Miyoshi, H. Makino, K. Matsumoto, H. Saito, S. Ogawa, Combination of hTERT and bmi-1, E6, or E7 induces prolongation of the life span of bone marrow stromal cells from an elderly donor without affecting their neurogenic potential, Mol. Cell Biol. 25 (2005) 5183–5195.

[24] S. Mimura, N. Kimura, M. Hirata, D. Tateyama, M. Hayashida, A. Umezawa, A. Kohara, H. Nikawa, T. Okamoto, M.K. Furue, Growth factor-defined culture medium for human mesenchymal stem cells, Int. J. Dev. Biol. 55 (2011) 181–187.

[25] K. Ishii, Y. Yoshida, Y. Akechi, T. Sakabe, R. Nishio, R. Ikeda, K. Terabayashi, Y. Matsumi, K. Gonda, H. Okamoto, Hepatic differentiation of human bone marrow–derived mesenchymal stem cells by tetracycline-regulated hepatocyte nuclear factor 3β, Hepatology 48 (2008) 597–606.

[26] J. Zhang, S. Yun, J. Bi, S. Dai, Y. Du, A.C. Zannettino, H. Zhang, Enhanced multi-lineage differentiation of human mesenchymal stem/stromal cells within poly (N-isopropylacrylamide-acrylic acid) microgel-formed three-dimensional constructs, J. Mater. Chem. B 6 (2018) 1799–1814.

[27] S. Senamontree, T. Lakthan, P. Charoenpanich, C. Chanchao, A. Charoenpanich, Betulinic acid decreases lipid accumulation in adipogenesis-induced human mesenchymal stem cells with upregulation of PGC-1α and UCP-1 and post-transcriptional downregulation of adiponectin and leptin secretion, PeerJ 9 (2021), e12321.

[28] H. Ishimine, N. Yamakawa, M. Sasao, M. Tadokoro, D. Kami, S. Komazaki, M. Tokuhara, H. Takada, Y. Ito, S. Kuno, N-Cadherin is a prospective cell surface marker of human mesenchymal stem cells that have high ability for cardiomyocyte differentiation, Biochem. Biophys. Res. Commun. 438 (2013) 753–759.

[29] E. Czekanska, M. Stoddart, R. Richards, J. Hayes, In search of an osteoblast cell model for in vitro research, Eur. Cell. Mater. 24 (2012) 1–17.

[30] S. Wilkesmann, J. Fellenberg, Q. Nawaz, B. Reible, A. Moghaddam, A.R. Boccaccini, F. Westhauser, Primary osteoblasts, osteoblast precursor cells or osteoblast-like cell lines: which human cell types are (most) suitable for characterizing 45S5-bioactive glass? J. Biomed. Mater. Res. 108 (2020) 663–674.

[31] S. Vohra, K.M. Hennessy, A.A. Sawyer, Y. Zhuo, S.L. Bellis, Comparison of mesenchymal stem cell and osteosarcoma cell adhesion to hydroxyapatite, J. Mater. Sci. Mater. Med. 19 (2008) 3567–3574.

[32] G. Bendas, L. Borsig, Cancer cell adhesion and metastasis: selectins, integrins, and the inhibitory potential of heparins, International Journal of Cell Biology (2012), 676731, https://doi.org/10.1155/2012/676731.

[33] M. Pierschbacher, S. Dedhar, E. Ruoslahti, S. Argraves, S. Suzuki, Year an adhesion variant of the MG-63 osteosarcoma cell line displays an osteoblast-like phenotype, in: Ciba Foundation Symposium 136-Cell and Molecular Biology of Vertebrate Hard Tissues: Cell and Molecular Biology of Vertebrate Hard Tissues: Ciba Foundation Symposium 136, Wiley Online Library, 2007, pp. 131–141.

[34] D. Docheva, D. Padula, C. Popov, W. Mutschler, H. Clausen-Schaumann, M. Schieker, Researching into the cellular shape, volume and elasticity of mesenchymal stem cells, osteoblasts and osteosarcoma cells by atomic force microscopy, J. Cell Mol. Med. 12 (2008) 537–552.

[35] F. Zhao, Q. Wu, X. Dai, Y. Li, H. Gan, R. Wang, J. Lv, Y. Chen, Programmed cell death 1 correlates with the occurrence and development of MG63 osteosarcoma, Oncol. Lett. 12 (2016) 5199–5204.

[36] S. Staehlke, H. Rebl, B. Nebe, Phenotypic stability of the human MG-63 osteoblastic cell line at different passages, Cell Biol. Int. 43 (2019) 22–32.

[37] R. Dwivedi, S. Kumar, R. Pandey, A. Mahajan, D. Nandana, D.S. Katti, D. Mehrotra, Polycaprolactone as biomaterial for bone scaffolds: review of literature, J. oral biology and craniofacial research 10 (2020) 381–388.

[38] H. Nekounam, M.R. Kandi, D. Shaterabadi, H. Samadian, N. Mahmoodi, E. Hasanzadeh, R. Faridi-Majidi, Silica nanoparticles-incorporated carbon nanofibers as bioactive biomaterial for bone tissue engineering, Diam. Relat. Mater. 115 (2021), 108320.

[39] L. Liu, H. Mu, Y. Pang, Caffeic acid treatment augments the cell proliferation, differentiation, and calcium mineralization in the human osteoblast-like MG-63 cells, Phcog. Mag. 17 (2021).

[40] S. Verma, N. Kumar, Effect of biomimetic 3D environment of an injectable polymeric scaffold on MG-63 osteoblastic-cell response, Mater. Sci. Eng. C 30 (2010) 1118–1128, https://doi.org/10.1016/j.msec.2010.06.005.

[41] C. Zhang, K. Ma, W.-Y. Li, IL-6 promotes cancer stemness and oncogenicity in U2OS and MG-63 osteosarcoma cells by upregulating the OPN-STAT3 pathway, J. Cancer 10 (2019) 6511.

[42] S. Lemos, B. Sampaio-Marques, P. Ludovico, I. Gaivão, C. Palmeira, G. Martins, F. Peixoto, R. Pinto-Leite, P. Oliveira, Elucidating the mechanisms of action of parecoxib in the MG-63 osteosarcoma cell line, Anti Cancer Drugs 31 (2020) 507–517.

[43] C.F. Marques, F.H. Perera, A. Marote, S. Ferreira, S.I. Vieira, S. Olhero, P. Miranda, J.M.F. Ferreira, Biphasic calcium phosphate scaffolds fabricated by direct write assembly: mechanical, anti-microbial and osteoblastic properties, J. Eur. Ceram. Soc. 37 (2017) 359–368, https://doi.org/10.1016/j.jeurceramsoc.2016.08.018.

[44] M. Varçin, B.B. Şener, C. Bayraç, Adsorption of resazurin by poly(acrylic acid) hydrogels and evaluation of its use in reduction assay for quantification of cell viability, Dyes Pigments 186 (2021), 109038, https://doi.org/10.1016/j.dyepig.2020.109038.

[45] K. Yang, Y. Zhao, X. Nie, H. Wu, B. Wang, C.M. Almodovar-Rivera, H. Xie, W. Tang, A cell-based target engagement assay for the identification of cereblon E3 ubiquitin ligase ligands and their application in HDAC6 degraders, Cell Chemical Biology 27 (2020) 866–876.e868, https://doi.org/10.1016/j.chembiol.2020.04.008.

[46] H.Y. Min, H.E. Son, W.G. Jang, Alpha-pinene promotes osteoblast differentiation and attenuates TNFα-induced inhibition of differentiation in MC3T3-E1 pre-osteoblasts, Clin. Exp. Pharmacol. Physiol. 47 (2020) 831–837.

[47] J. Jeong, H. Park, H. Hyun, J. Kim, H. Kim, H.I. Oh, H.S. Hwang, D.K. Kim, H.H. Kim, Effects of glucosinolates from turnip (Brassica rapa L.) root on bone formation by human osteoblast-like MG-63 cells and in normal young rats, Phytother Res. 29 (2015) 902–909.

[48] S.E. Kim, Y.-P. Yun, J.Y. Lee, K. Park, D.H. Suh, Osteoblast activity of MG-63 cells is enhanced by growth on a lactoferrin-immobilized titanium substrate, Colloids Surf. B Biointerfaces 123 (2014) 191–198, https://doi.org/10.1016/j.colsurfb.2014.09.014.

[49] N. Fani, M. Farokhi, M. Azami, A. Kamali, N.L. Bakhshaiesh, S. Ebrahimi-Barough, J. Ai, M.B. Eslaminejad, Endothelial and osteoblast differentiation of adipose-derived mesenchymal stem cells using a cobalt-doped CaP/silk fibroin scaffold, ACS Biomater. Sci. Eng. 5 (2019) 2134–2146, https://doi.org/10.1021/acsbiomaterials.8b01372.

[50] A. Brauer, T. Pohlemann, W. Metzger, Osteogenic differentiation of immature osteoblasts: interplay of cell culture media and supplements, Biotech. Histochem. 91 (2016) 161–169, https://doi.org/10.3109/10520295.2015.1110254.

[51] J.T.Y. Lee, K.L. Chow, SEM sample preparation for cells on 3D scaffolds by freeze-drying and HMDS, Scanning 34 (2012) 12–25.

[52] H. Heremans, A. Billiau, J.J. Cassiman, J.C. Mulier, P. de Somer, Vitro cultivation of human tumor tissues II. Morphological and virological characterization of three cell lines, Oncology 35 (1978) 246–252, https://doi.org/10.1159/000225298.

[53] D. Lajeunesse, C. Frondoza, B. Schoffield, B. Sacktor, Osteocalcin secretion by the human osteosarcoma cell line MG-63, J. Bone Miner. Res. 5 (1990) 915–922.

[54] M. Abdulwahab, A.A. Khan, S.H. Abdallah, M.N.K. Khattak, B. Workie, M.M. Chehimi, A.A. Mohamed, Arylated gold nanoparticles have no effect on the adipogenic differentiation of MG-63 cells nor regulate any key signaling pathway during the differentiation, BMC Res. Notes 14 (2021) 1–7.

[55] S. Fukumoto, T. Fujimoto, Deformation of lipid droplets in fixed samples, Histochem. Cell Biol. 118 (2002) 423–428.

[56] A.T. El-Serafi, D. Sandeep, S. Abdallah, Y. Lozansson, M. Hamad, A.A. Khan, Paradoxical effects of the epigenetic modifiers 5-aza-deoxycytidine and suberoylanilide hydroxamic acid on adipogenesis, Differentiation 106 (2019) 1–8.

[57] J.A. Olzmann, P. Carvalho, Dynamics and functions of lipid droplets, Nat. Rev. Mol. Cell Biol. 20 (2019) 137–155.

[58] N. Leitner, J. Hlavatý, R. Ertl, S. Gabner, A. Fuchs-Baumgartinger, I. Walter, Lipid droplets and perilipins in canine osteosarcoma. Investigations on tumor tissue, 2D and 3D cell culture models, Vet. Res. Commun. (2022) 1–19.

[59] J. Roy, P. Dibaeinia, T.M. Fan, S. Sinha, A. Das, Global analysis of osteosarcoma lipidomes reveal altered lipid profiles in metastatic versus nonmetastatic cells [S], J. Lipid Res. 60 (2019) 375–387.

[60] A. Royo-García, S. Courtois, B. Parejo-Alonso, P. Espiau-Romera, P. Sancho, Lipid droplets as metabolic determinants for stemness and chemoresistance in cancer, World J. Stem Cell. 13 (2021) 1307.

[61] N.A. Twine, L. Chen, C.N. Pang, M.R. Wilkins, M. Kassem, Identification of differentiation-stage specific markers that define the ex vivo osteoblastic phenotype, Bone 67 (2014) 23–32.

[62] L. Xu, Y. Liu, Y. Sun, B. Wang, Y. Xiong, W. Lin, Q. Wei, H. Wang, W. He, B. Wang, et al., Tissue source determines the differentiation potentials of mesenchymal stem cells: a comparative study of human mesenchymal stem cells from bone marrow and adipose tissue, Stem Cell Res. Ther. 8 (2017) 275, https://doi.org/10.1186/s13287-017-0716-x.

[63] C. Ulrich, B. Rolauffs, H. Abele, M. Bonin, K. Nieselt, M.L. Hart, W.K. Aicher, Low osteogenic differentiation potential of placenta-derived mesenchymal stromal cells correlates with low expression of the transcription factors Runx2 and Twist2, Stem Cell. Dev. 22 (2013) 2859–2872.

[64] J. Delgado-Calle, C. Sañudo, L. Sánchez-Verde, R.J. García-Renedo, J. Arozamena, J.A. Riancho, Epigenetic regulation of alkaline phosphatase in human cells of the osteoblastic lineage, Bone 49 (2011) 830–838.

[65] C.A. Gregory, A.S. Perry, E. Reyes, A. Conley, W.G. Gunn, D.J. Prockop, Dkk-1-derived synthetic peptides and lithium chloride for the control and recovery of adult stem cells from bone marrow, J. Biol. Chem. 280 (2005) 2309–2323.

[66] W. Qiu, T.E. Andersen, J. Bollerslev, S. Mandrup, B.M. Abdallah, M. Kassem, Patients with high bone mass phenotype exhibit enhanced osteoblast differentiation and inhibition of adipogenesis of human mesenchymal stem cells, J. Bone Miner. Res. 22 (2007) 1720–1731.

[67] J.E. Aubin, Advances in the osteoblast lineage, Biochem. Cell. Biol. 76 (1998) 899–910.

[68] L.L. McManus, F. Bonnier, G.A. Burke, B.J. Meenan, A.R. Boyd, H.J. Byrne, Assessment of an osteoblast-like cell line as a model for human primary osteoblasts using Raman spectroscopy, Analyst 137 (2012) 1559–1569.

[69] M. Tzaphlidou, V. Zaichick, Calcium, phosphorus, calcium-phosphorus ratio in rib bone of healthy humans, Biol. Trace Elem. Res. 93 (2003) 63–74.

[70] H. Mitchell, T. Hamilton, F. Steggerda, H. Bean, The chemical composition of the adult human body and its bearing on the biochemistry of growth, J. Biol. Chem. 158 (1945) 625–637.

[71] L.M. Schäck, S. Noack, R. Winkler, G. Wißmann, P. Behrens, M. Wellmann, M. Jagodzinski, C. Krettek, A. Hoffmann, The phosphate source influences gene expression and quality of mineralization during in vitro osteogenic differentiation of human mesenchymal stem cells, PLoS One 8 (2013), e65943, https://doi.org/10.1371/journal.pone.0065943.

[72] F. Lamonaca, M. Vasile, A. Nastro, Measurement method for the objective and early detection of the osteosarcoma tumors, Measurement 92 (2016) 89–95.

[73] J. Tang, Q. Xie, G. Pan, J. Wang, M. Wang, Mesenchymal stem cells participate in angiogenesis and improve heart function in rat model of myocardial ischemia with reperfusion, Eur. J. Cardio. Thorac. Surg. 30 (2006) 353–361.

[74] A. Wofford, A. Bow, S. Newby, S. Brooks, R. Rodriguez, T. Masi, S. Stephenson, J. Gotcher, D.E. Anderson, J. Campbell, Human fat-derived mesenchymal stem cells xenogenically implanted in a rat model show enhanced new bone formation in maxillary alveolar tooth defects, Stem Cell. Int. (2020).

[75] C. Zhang, D. Xia, J. Li, Y. Zheng, B. Weng, H. Mao, J. Mei, T. Wu, M. Li, J. Zhao, BMSCs and osteoblast-engineered ECM synergetically promotes osteogenesis and angiogenesis in an ectopic bone formation model, Front. Bioeng. Biotechnol. 10 (2022) 12.

[76] M. Kim, K.H. Kim, S.U. Song, T.G. Yi, S.H. Yoon, S.R. Park, B.H. Choi, Transplantation of human bone marrow-derived clonal mesenchymal stem cells reduces fibrotic scar formation in a rat spinal cord injury model, Journal of Tissue Engineering and Regenerative Medicine 12 (2018) e1034–e1045.

[77] V. Egea, K. Kessenbrock, D. Lawson, A. Bartelt, C. Weber, C. Ries, Let-7f miRNA regulates SDF-1α-and hypoxia-promoted migration of mesenchymal stem cells and attenuates mammary tumor growth upon exosomal release, Cell Death Dis. 12 (2021) 516.

[78] D.S. Chulpanova, K.V. Kitaeva, L.G. Tazetdinova, V. James, A.A. Rizvanov, V.V. Solovyeva, Application of mesenchymal stem cells for therapeutic agent delivery in anti-tumor treatment, Front. Pharmacol. 9 (2018) 259.

[79] J.-L. Yu, S. Chan, M.K.-L. Fung, G.C.-F. Chan, Mesenchymal stem cells accelerated growth and metastasis of neuroblastoma and preferentially homed towards both primary and metastatic loci in orthotopic neuroblastoma model, BMC Cancer 21 (2021) 1–12.

[80] J. Chen, T. Ji, D. Wu, S. Jiang, J. Zhao, H. Lin, X. Cai, Human mesenchymal stem cells promote tumor growth via MAPK pathway and metastasis by epithelial mesenchymal transition and integrin α5 in hepatocellular carcinoma, Cell Death Dis. 10 (2019) 425, https://doi.org/10.1038/s41419-019-1622-1.

[81] A. Moya, J. Paquet, M. Deschepper, N. Larochette, K. Oudina, C. Denoeud, M. Bensidhoum, D. Logeart-Avramoglou, H. Petite, Human mesenchymal stem cell failure to adapt to glucose shortage and rapidly use intracellular energy reserves through glycolysis explains poor cell survival after implantation, Stem Cell. 36 (2018) 363–376.

[82] M. Muñoz, M. Berger, M. Rosso, A. Gonzalez-Ortega, A. Carranza, R. Coveñas, Antitumor activity of neurokinin-1 receptor antagonists in MG-63 human osteosarcoma xenografts, Int. J. Oncol. 44 (2014) 137–146.

[83] Y. Dai, H. Liu, B. Liu, Z. Wang, Y. Li, G. Zhou, Porous β-Ca2SiO4 ceramic scaffolds for bone tissue engineering: in vitro and in vivo characterization, Ceram. Int. 41 (2015) 5894–5902.

[84] S.-R. Son, N.-T.B. Linh, H.-M. Yang, B.-T. Lee, Vitro and in vivo evaluation of electrospun PCL/PMMA fibrous scaffolds for bone regeneration, Sci. Technol. Adv. Mater. 14 (2013), 015009, https://doi.org/10.1088/1468-6996/14/1/015009.